Geophysical Journal International

Geophys. J. Int. (2009) **179,** 1859–1869 doi: 10.1111/j.1365-246X.2009.04391.x

Two-station measurement of Rayleigh-wave phase velocities for the Huatung basin, the westernmost Philippine Sea, with OBS: implications for regional tectonics

Ban-Yuan Kuo,[1] Wu-Cheng Chi,[1] Ching-Ren Lin,[1,2] Emmy Tsui-Yu Chang,[3] John Collins[4] and Char-Shine Liu[3]

[1] *Institute of Earth Sciences, Academia Sinica, Taipei, Taiwan. E-mail: byk@earth.sinica.edu.tw*
[2] *Institute of Geophysics, National Central University, Chung-Li, Taiwan*
[3] *Institute of Oceanography, National Taiwan University, Taipei, Taiwan*
[4] *Department of Geology and Geophysics, Woods Hole Oceanographic Institution, Woods Hole,* MA 02543, *USA*

Accepted 2009 September 20. Received 2009 September 20; in original form 2008 July 19

SUMMARY

A broad-band ocean-bottom seismometer (OBS) deployed ∼180 km east of Taiwan provides a first glimpse into the upper mantle beneath the westernmost section of the Philippine Sea or the Huatung basin (HB). We measured interstation phase velocities of Rayleigh waves between the OBS and stations on the eastern coast of Taiwan. The phase velocities show smooth variations from 3.8 to 3.9 km s^{-1} for periods of 25–40 s. In this short period range, phase velocities are comparable to those characterizing the 15–30 Ma Parece-Vela basin of the Philippine Sea. Modelling of the finite-frequency effect proves the validity of the measurement for the average HB. The shear-wave velocity models inverted from the 25 to 40 s dispersion show a velocity at lithospheric depths about 0.1 km s^{-1} lower than that of the west Philippine Sea, which agrees with the age effect derived from the Pacific pure-path model. Inversions incorporating the less reliable data above 40 s yield a shear velocity <4.0 km s^{-1} below 150 km, an unrealistic value even for a hotspot plume environment. The seismological evidence, together with the correlation in seafloor depth, suggests that the HB and the Parece-Vela basin may have a similar age. This is at odds with the previous geochronological study suggesting an early-Cretaceous age for the HB. Thermal rejuvenation of the lithosphere was examined as a potential solution to reconciling the two age models.

Key words: Surface waves and free oscillations; Wave propagation; Continental margins: convergent; Dynamics of lithosphere and mantle.

1 INTRODUCTION

The origin of the west Philippine basin (WPB), the region of the Philippine Sea basin to the west of the Palau-Kyushu ridge, has been intensively but inconclusively discussed for decades. One hypothesis involves trapping of a piece of normal oceanic plate after the Pacific Plate changed its absolute motion direction in the early Tertiary (Hilde & Lee 1984; Jolivet *et al.* 1989). Other models, backed by detailed studies of seafloor morphology and plate reconstruction, prefer a backarc basin related origin (Lee & Lawver 1995; Okino *et al.* 1999; Deschamps & Lallemand 2002). While investigators are split in their view on the overall evolution of the basin, they generally agree on the age of the WPB to be roughly from 30 to 60 Ma and treat them as a fixed parameter in pursuit of interpretations (e.g. Hall *et al.* 1995). Recently, a new issue arose garnering much attention which involved a large disparity in the age determination concerning the westernmost section of the WPB, Huatung basin (HB). This disparity, if unresolved, will further add to the difficulty in unraveling the evolutionary history of both the HB and the WPB.

Occupying the westernmost corner of the WPB and to the west of the Gagua ridge (GR), the HB is a small piece of oceanic lithosphere directly engaged in the subduction-collision processes in the Taiwan region (Fig. 1). Most palaeomagnetic studies in the past portrayed the HB to be the younger counterpart (∼40 Ma) of the neighbouring WPB (∼50 Ma), separated by a north–south oriented fracture zone known today as the GR (e.g. Hilde & Lee 1984). Based on Ar–Ar dating and palaeontological evidence, however, Deschamps *et al.* (2000) suggested that the HB was generated in the early Cretaceous (∼125 Ma) and trapped by the Philippine Sea plate (PSP) during the northward migration of the latter. The new age assignment not only reverses the sense of the age contrast across the GR but also increases the magnitude of the contrast by ∼70 Myr.

Despite the potential impact of this issue in regional tectonics, independent seismological characterizations of the HB have been absent in the past due to the basin's small size and the difficulty

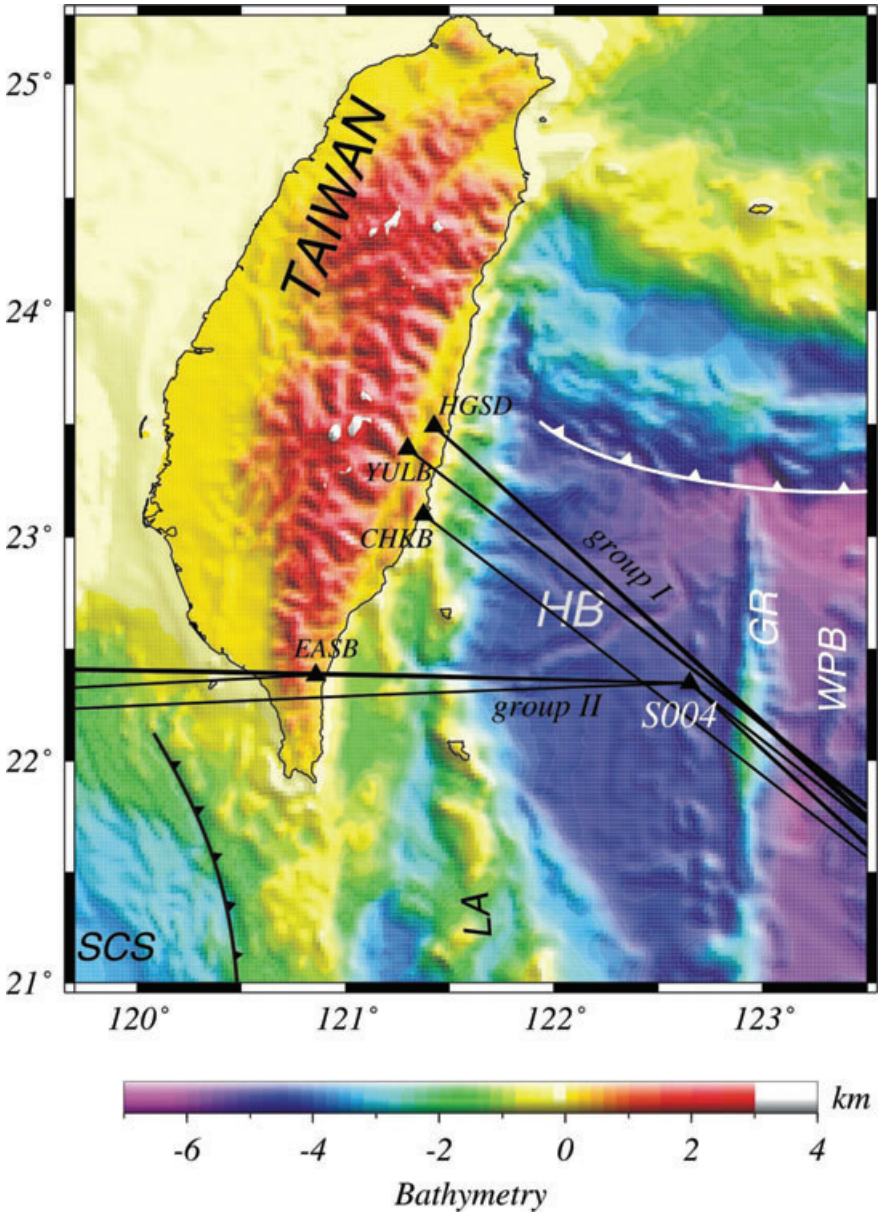

Figure 1. Map of the region of Taiwan and the Huatung basin (HB) in the westernmost Philippine Sea, showing relevant tectonic elements and great-circle paths of Rayleigh waves and station names used in this study. S004 is the OBS station. Group I refers to the five pairs of paths to S004 and HGSD, YULB and CHKB, and group II refers to the three pairs of paths to EASB and S004. GR: Gagua ridge; SCS: South-China Sea; LA: Luzon arc; WPB: western Philippine basin. The sawtooth denotes the Ryukyu (white) trench and the Manila (black) trench.

in sampling it from the open ocean. Previous studies have mapped the PSP upper mantle mainly using seismic stations on the border, rendering a regional resolution (>1000 km) that either completely misses the HB or does not distinguish the HB from the WPB (Oda & Senna 1994; Nakamura & Shibutani 1998; Kato & Jordan 1999). Recently, a large amount of ocean-bottom seismometer (OBS) data were utilized to map the Philippine Sea upper mantle, but the HB was again not covered independently (e.g. Isse *et al.* 2004). In this study, we take advantage of one broad-band OBS deployed near the eastern margin of the HB, slightly west of the GR (station S004, Fig. 1), to achieve the observation aperture necessary to illuminate the basin in an *in situ* manner. This opportunity is rare because in the foreseeable future no deployments are planned to fully cover the breadth of the basin. OBS deployments in the middle of the HB entail too small a distance for Rayleigh wave measurement aimed at lithospheric structures. The single station S004 paired with the land stations on Taiwan prove to be capable of providing independent constraints on the properties and shedding new light on the tectonic evolution of the HB.

2 DATA AND MEASUREMENT

The OBS was deployed on the seafloor at 4726 m and estimated to be located to within ∼200 m based on a boot-strap relocation practice. The instrument is equipped with a sensor which has a flat velocity response from 20 Hz to 120 s and is levelled by a gimbal (e.g. Collins *et al.* 2001; Lin *et al.* 2009). The sensor, housed in an aluminum ball, is anchored on the seafloor by its own weight without burial into the sediment, but high-quality waveforms have been

Table 1. Event list.

No.	Date/time[a]	lat	lon	z	baz1[b]	baz2[b]	Δ[c]	Group
1	2006.290.01.25:12.23 (10/17)	−5.88	150.98	32	132.01(s004)	131.65(hgsd)	39.44	I
2	2006.311.17.38:33.63 (11/07)	−6.48	151.20	10	132.41(s004)	132.03(hgsd)	40.03	I
3	2006.317.16.12:28.98 (11/13)	−6.38	151.23	11	132.27(s004)	131.90(hgsd)	39.98	I
4	2007.092.10.49:17.72 (04/02)	−7.22	156.24	34	127.94(s004)	127.48(yulb) 127.33(chkb)	44.11	I
5	2007.136.08.56:16.47 (05/16)	20.50	100.75	24	268.04(easb)	268.94(s004)	20.47	II
6	2007.174.08.17:19.89 (06/23)	21.47	99.78	22	271.33(easb)	271.97(s004)	21.23	II
7	2007.211.22.42:05.63 (07/30)	19.31	95.61	14	267.28(easb)	268.18(s004)	25.44	II

[a]Event data/time is given as a julian year, day, hour, minute (delimited by a dot) and second (following a semi column). In parenthesis is month/day.
[b]baz1: backazimuth at station 1; baz2: backazimuth at station 2.
[c]Great-circle arc distance to station 1.

recorded on the vertical component. The records were corrected for the clock-drift of ∼0.34 s in 350 d. We carried out an interstation phase velocity measurement of Rayleigh waves between S004 and the land-based stations. The geometrical criterion for a valid two-station measurement is a small deviation of the interstation great-circle path from the great-circle path at either station. In this study, this deviations are 1–5°, comparable to that (2–6°) in the study of Hawaii-Oahu hotspot chain (Priestley & Tilmann 1999) but larger than the 3° criterion used in Yao *et al.* (2006) with a fully 3-D network.

We obtained two groups of paths suitable for a two-station measurement: group I between S004 and land stations HGSD, YULB or CHKB, and group II between EASB and S004 (Fig. 1). Event information is listed in Table 1. The interstation distances, taken to be the difference between the epicentral distances of the two stations, are approximately 178 and 182 km for groups I and II, respectively. Instrument responses were deconvolved from the waveforms at both S004 and land stations to yield displacements. The Rayleigh-wave waveforms are prominent in group I (Fig. 2) and less prominent in group II due to a noisier ocean-bottom environment in 2007, a short propagation range, and probable interference by more complicated structures along the paths.

We employed the cross-correlation method after Bloch & Hales (1968) to determine the phase velocity between stations. All seismograms were first windowed between 50 s before 4 and 2.5 $\mathrm{km\,s^{-1}}$ to remove obvious body wave phases before the Rayleigh wave fundamental mode and the coda after it. We determined the group arrival time for each record using a multiple-filter technique (Landisman *et al*. 1969). Each seismogram is then windowed with a flat plateau three-period long centred at the apparent group arrival time and a cosine taper one-period long on either end. The isolated energy is next subjected to a narrow-band filtering centred at the target frequency. The length between the corner of the filter and the central frequency is 1/20 of the period of interest. The nearly single-frequency harmonic waves for the two pairing stations were cross-correlated to yield a series of peaks that indicate potential interstation phase velocities. The final step of the measurement sequence involves mapping the cross-correlation functions to velocity, using a cubic-spline interpolation (e.g. Yao *et al.* 2006). A valid determination usually produces a smooth, continuous dispersion curve. In this study, group velocity dispersions often exhibit a rapid change, if not a jump, at periods <25 s at the land stations in group I, which is probably caused by the large topographic gradient across the east coast of Taiwan. This gives rise to discontinuities in interstation phase-velocity. The 2π ambiguity can be eliminated readily by imposing an acceptable velocity range.

Interferences from multipathing, higher modes and body waves that were hard to remove manually were examined by performing phase-matched filtering (Herrin & Goforth 1977) using the code after Herrmann & Ammon (2004). The 4–2.5 $\mathrm{km\,s^{-1}}$ windowing in the original routine is replaced by this step. In group I, phase-matched filtering gives essentially the same result as without it. For group II, body waves are too close to the fundamental mode because of the shorter epicentral distances and multipathing is suspected to affect the Rayleigh wave train. These undesired signals have been suppressed by the phase-matched filter. As a result, the consistency of the measurements in group II was improved, although not to the level of group I. All original waveforms of group I and the fundamental modes extracted by the phase-matched filter for group II are shown in Fig. 2.

We attained five successful measurements for group I and 3 for group II, respectively (Fig. 3). The scatters in both groups at short periods result from the discontinuities in group arrivals mentioned above. The divergence at longer periods reflects deteriorating accuracy when the wavelength approaches the interstation distance. We first choose 25 s as the lower bound and 40 s as the upper bound of the periods for reliable measurement. Later we relax the upper limit to 50 s, and reach the inference that the longer period measurements are probably unreliable. Within the 25–40 s band, the group I phase velocities increase from 3.8 to 3.9 $\mathrm{km\,s^{-1}}$, almost monotonically (Fig. 3). Group II velocities are substantially variable in the same period range and much lower than the velocities of group I. These significantly low velocities may be attributed to the travel of Rayleigh waves partly in the mantle wedge above the South-China Sea oceanic slab subducted under the Manila trench (Fig. 1). This mantle wedge environment may mask the real properties of the HB lithosphere. Due to this and the fact that both the number and quality of waveforms in group II are relatively low, we neglect group II in the present study and will focus our interpretation only on the group I data which are more accurately determined and representative of the HB.

The mean of the five dispersion data of group I is used to represent typical HB. Twice of the standard error of the mean at each period is used to represent the 95 per cent confidence interval. The consistency in measurements as indicated by the small 95 per cent interval is comparable to that in previous two-station measurements (Woods & Okal 1996; Priestley & Tilmann 1999). The group I means are compared with the pure-path velocities for various age zones of the Pacific basin (Nishimura & Forsyth 1988) in Fig. 4. The means are for the most part below that of the Pacific 4–20 Ma age zone. When compared with other tectonic provinces of the PSP itself, group I is to the first order consistent with the Parece-Vela basin (PVB) of 15–30 Ma (Isse *et al.* 2004). This observation is

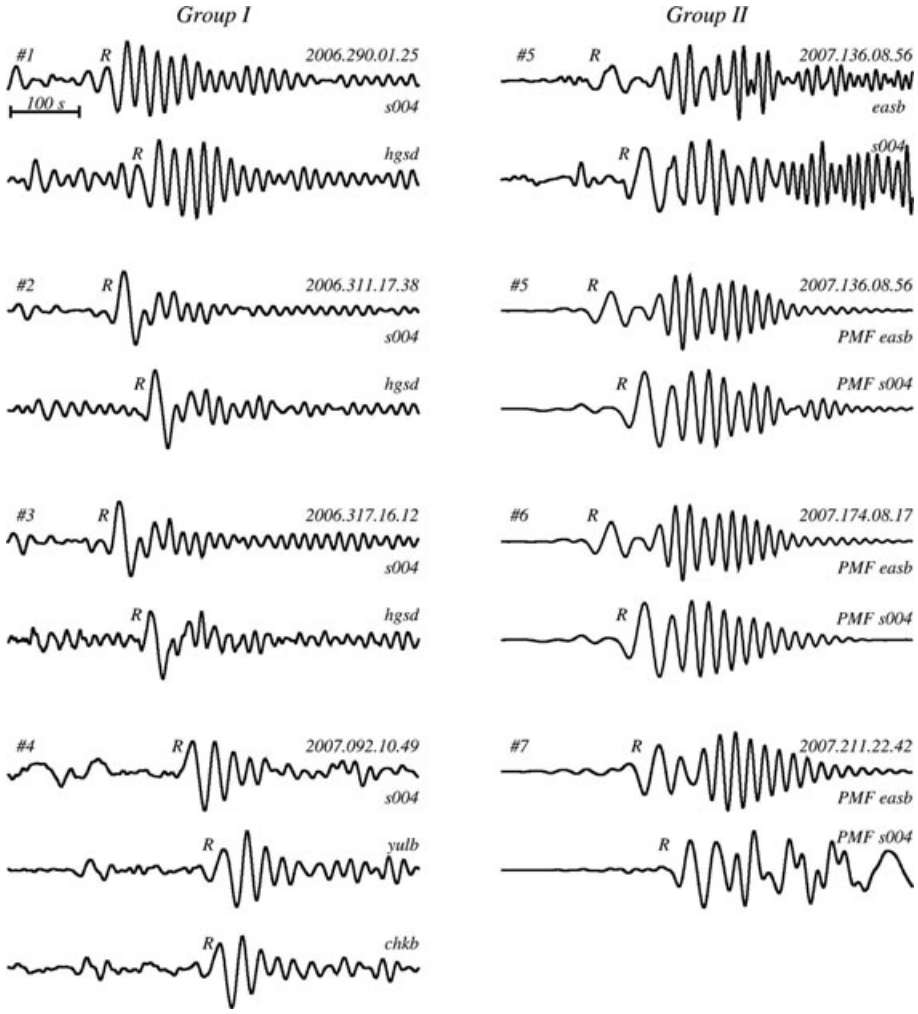

Figure 2. Waveforms of Rayleigh waves on vertical-component records of the station pairs used for the two-station measurement, bandpass filtered between 0.01 and 0.1 Hz for a better illustration. Left column: Group I; 5 pairs of original waveforms. Right column: Group II; first pair is an example of the original waveform, and the following 3 pairs are phase-matched filtered waveforms of all the three pairs (labeled *PMF*). Each pair of waveforms is denoted by the event number (Table 1), date/time (year, Julian day, hour and minute) and station name. *R* marks the arrival of Rayleigh waves. Group I is of higher quality than group II.

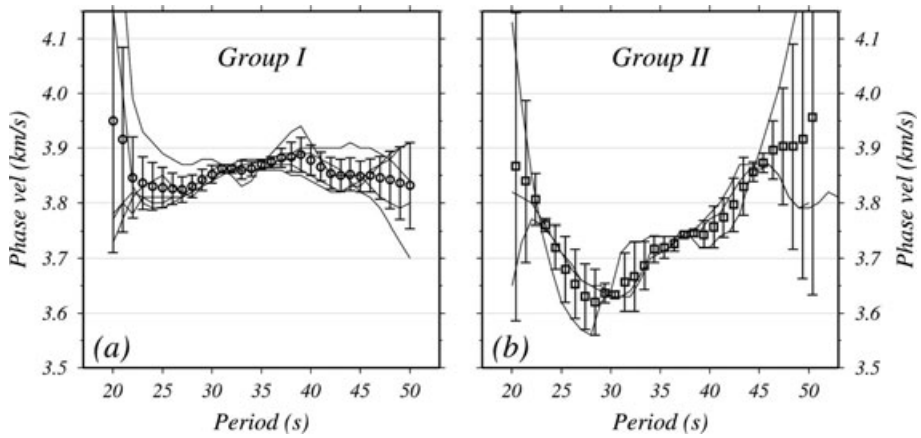

Figure 3. Individual measurements of phase velocities (thin, solid lines) for each event in (a) group I and (b) group II. Superimposed are means (circles and squares) and the twice of the standard errors of the means (bars) or approximately the 95 per cent confidence interval. Note the scatters at short and long periods. Measurements are deemed reliable in the band 25–40 s.

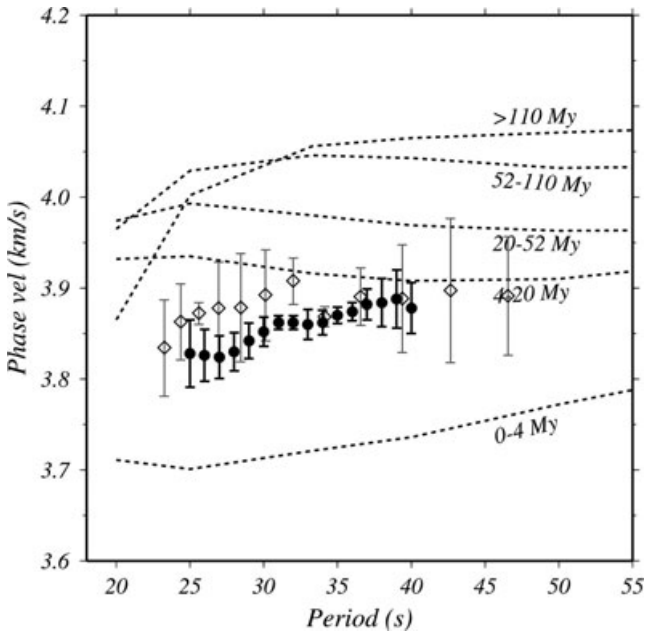

Figure 4. Means and 2 standard-error bars of the phase velocities in the period range of 25–40 s for groups I (filled circle), compared with the phase velocities for the Parece-Vela basin (PVB) (open diamond) which has an age of 15–30 Ma (Isse *et al.* 2004). The pure-path velocities for various Pacific age zones (Nishimura & Forsyth 1988) (dotted lines) are shown to illustrate the generally recognized base-line shift in velocity between the Pacific and the marginal seas.

compatible with the general understanding that the marginal sea is lower in velocity than the open oceanic basins, with a base-line offset of 0.05–0.1 km s^{-1}. Hereafter the PVB velocities, instead of the Pacific velocities, are the reference for discussion on the implications of the HB observations. Because the age of the PVB has been determined relatively well to be 15–30 Ma (Okino *et al.* 1998; Sdrolias *et al.* 2004), the general agreement in phase velocities between group I and the PVB highlights the potential contradiction between this study and Deschamps *et al.* (2000) in which the HB is assigned an age of ∼125 Ma.

3 FINITE-FREQUENCY EFFECT

In the limit of ray, the two-station method eliminates the effect of heterogeneity between the event and the nearer station and focuses sensitivity along the geometrical ray path between the two stations. However, the waveform of Rayleigh wave is composed of finite frequencies and its construction could be contributed from diffraction from heterogeneities over a broad region so that the ray-based two-station method may be invalid (e.g. Spetzler *et al.* 2002). To test the finite-frequency effect, we calculate the 2-D phase-velocity kernel formulated by Spetzler *et al.* (2002) for event 3 of group I (Table 1; see Fig. 2, event label 2006.317.16.12). The finite-frequency kernel in Spetzler *et al.* (2002) was originally formulated for observables such as relative phaseshift or traveltime residual (δt) with respect to local phase velocity perturbations (δc). Here we express the kernel explicitly as the sensitivity of measured phase velocity perturbation $\delta v/v$ with respect to $\delta c/c$ via the first order equity $\delta v/v = -\delta t/t$, where v (or c) is the reference phase velocity and t is the reference traveltime. Because the waveforms were windowed around the group arrival time for cross-correlation, the kernels have to be further smoothed over the range of frequencies corresponding to this time-domain window (Yang & Forsyth 2006). For the event used, the radiation pattern of the source can be ignored. The kernels for 40 s and a v of 4 km s^{-1} at station 1 (e.g. S004) and station 2 (e.g. HGSD), K_1 and K_2, are shown in Figs 5(a) and (b), respectively. The kernel for the interstation $\delta v/v$ is not just the difference between K_2 and K_1 but instead constructed as

$$\delta K = K_2 \frac{t_2}{t_2 - t_1} - K_1 \frac{t_1}{t_2 - t_1}, \tag{1}$$

where t_1 and t_2 are traveltimes of Rayleigh waves for stations 1 and 2, respectively (Fig. 5c). Because the kernel associated with each single station is highly skewed towards both ends, eq. (1) leaves significant negative kernels in the wake of station 1 (S004), although δK in the vicinity of the source mostly vanishes. Integration of (1) with $\delta c/c$ yields the predicted interstation $\delta v/v$

$$\frac{\delta v}{v} = \int_0^{\Delta} \int_0^{\pi} \delta K \frac{\delta c}{c} \, \mathrm{d}\theta \mathrm{d}\phi, \tag{2}$$

where θ is colatitude and ϕ is longitude when the event-station is rotated to parallel the equator and Δ is the epicentral distance of station 2. Note δv is the observable, that is, the interstation phase velocity perturbation measured, and δc is the potential contributor to δv.

Because eq. (1) is presented for the first time, we examine with examples on how an anomaly source-side of station 1 could 'leak' to the interstation velocity. First, we explore the maximum effect of leakage by placing a circular anomaly of 85 km in radius to encompass most of the negative kernel east of station 1 (Fig. 5c, dotted circle). Eq. (2) is evaluated with this $\delta c/c$ to predict an apparent $\delta v/v$. With this configuration a 0.1 km s^{-1} δc contributes a -0.032 km s^{-1} to δv, which would of course lead to the erroneous interpretation that shear-wave velocity V_S is reduced in the media between the two stations. As a check, the same anomaly ($\delta c = 0.1$ km s^{-1}) placed to cover the positive kernel fully between the two stations (Fig. 5c, dashed circle) contributes a δv of 0.1 km s^{-1} correctly. This example illustrates that, in a statistical sense, the relative importance of the source-side anomaly could be as much as $-1/3$ of that between the stations for the anomaly of the same size.

The tests above verify the formulation in (2), but are irrelevant to the tectonic context of this region. A more likely scenario of systematic leakage in this region may stem from the difference between the WPB and the HB. The inversion described in the next section suggests that the WPB is probably 0.1 km s^{-1} faster in V_S than the HB. Here we test if this possible systematic difference, equivalent to a $\delta c \sim 0.07$ km s^{-1} if the V_S perturbation is distributed in upper 100 km depths, can bias the interstation measurements. In the calculation the WPB and HB are separated by the GR (Fig. 5c), which is thought to be a remnant fracture zone (Deschamps *et al.* 1998). Integration of (1) over this model, that is, $\delta c = 0$ for HB and 0.07 km s^{-1} for WPB, yields a δv of -0.003 km s^{-1}. This leakage can be ignored as a small error. We conclude that the group I phase velocities primarily detect the upper mantle of the HB, without significant bias from the WPB.

Because the sensitivity is skewed towards HGSD, the possibility exists that a strongly negative anomaly in the vicinity of HGSD contributes to the apparently low average of HB. The upper mantle beneath Taiwan has not been imaged well enough to provide a direct answer to this possibility. Based on a forward modelling of traveltime and amplitude, Chen *et al.* (2004) propose the presence of a continuously subducted slab in the upper mantle beneath central Taiwan, which implies exactly the opposite to the above possibility. In another scenario, if the slab detached, the associated return flow may heat up the asthenosphere leading to low velocities. However,

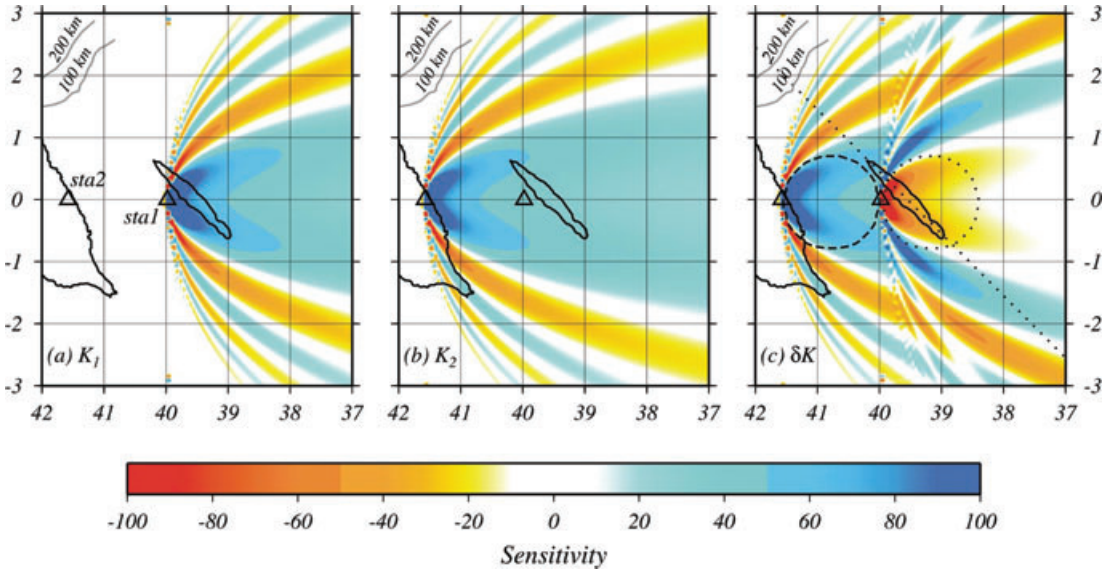

Figure 5. Sensitivities of Rayleigh wave phase velocity observation $\delta v/v$ with respect to local perturbation $\delta c/c$, (a) at station 1 (S004) at $\Delta = 40^{o}$ and (b) at station 2 (HGSD) at $\Delta = 41.6^{o}$ and (c) for between the two stations. This example may apply to all data of group I. The centre period is 40 s. Coordinate frame is rotated to align the great-circle path along the equator. Gray lines on the upper-left corner are depth contours of the subducted slab of the PSP (Chou *et al.* 2006) to show they are too far to make contributions. In (c), dotted and dashed circles outline the local phase velocity perturbations δc of 0.1 km s^{-1} tested in the text, which give rise to -0.032 km s^{-1} (leakage) and 0.1 km s^{-1} for interstation velocity δv, respectively. The straight dotted line passing through the GR outlined by the 4500-m contour represents the boundary between the HB on the lower-left and the WPB on the upper right.

this upwelling is usually perceived to be wide spreading rather than localized. To further appraise the effect of the localized anomaly, we put a circular, negative δc spanning the northwest 1/3 of the interstation distance with its border abutting HGSD. Now we treat the above 0.07 km s^{-1} as the observable, and assume that the HB measurement is biased by a δv of -0.07 km s^{-1} relative to the WPB. To obtain such a δv, eq. (2) requires that δc be -0.3 km s^{-1} in the designated circular region, or equivalently a V_S decrease of $\sim$0.4 km s^{-1} over lithospheric depths. If this decrease in V_S is thermal, the temperature increase will be as unreasonably large as $\sim$900^{o}C using a coefficient of -0.00045 km s^{-1} per degree (Song & Helmberger 2007). In addition, no topographic expression is observed in this area that can be related to this hypothetical thermal anomaly. We find no particular reason to suspect that the observed low velocity for the HB results from a significantly low velocity regime in the northwest section of the interstation region. The effect of a thick crust along the eastern coast of Taiwan is evaluated in the next section.

4 INVERSION

The phase-velocity data of group I were inverted to path-average V_S model using the algorithm developed by Thomson (1997). The interstation distance is only $\sim$178 km, compared with the distances of 360 and 2100 km in Priestley & Tilmann (1999) and Woods & Okal (1996), respectively that employed the two-station method to characterize the upper mantle of the Hawaiian hotspot chain. In those two studies reliable measurements were extended to 80 s with resolvable depths to 200 km. The narrow bandwidth (25–40 s) of the dispersion we first target together with the actual $\sim$10 s period resolution warrant probably only resolving uniform velocities over lithospheric depths. Nevertheless, we carried out an inversion for the upper 150 km with a model prescribed to 250 km depth discretized into 20–50-km-thick layers and allow the regularization scheme of inversion to dictate the model configuration. The crustal structure of the HB has been investigated using high-frequency OBS and multichannel seismic refraction data (Wang *et al.* 2004; McIntosh *et al.* 2005). While the crust may be thicker near the coast, it is 'normal' with a thickness $h < 10$ km in the HB. We first test a 10 km crust with a 5 km water column representing much of the Rayleigh wave interstation path. The initial model has 3.3 km s^{-1} for oceanic crust, 4.3 km s^{-1} for mantle to 150 km and 4.4 km s^{-1} below, which provides 88 per cent variance reduction of the data. For the purpose of this study, however, we did not take into account the number of model parameters in calculating the variance.

The non-uniqueness of the inversion can be fully appreciated by examining the trade-off between a model's ability to explain data and the 'cost' of that ability, that is, the uncertainty of the model parameters. To estimate the latter, we performed a large set of inversions ($\sim$200) with data contaminated by random errors that are statistically consistent with the standard errors of the group I means. Each inversion is regularized through an a priori model variance given to the covariance matrix and a correlation coefficient of 0.3 between adjacent layers. The 'model error' is taken to be the average of the standard deviations of V_S of all layers below the crust and above 150 km. The trade-off curve is constructed as the variance reduction of data as a function of the model error.

Fig. 6 presents two example models of HB with $h = 10$ km chosen from separate points on the trade-off curve. The optimal model (A) from a trade-off point of view provides a variance reduction of 92 per cent with small model error $\sim$0.003 km s^{-1}. The heavy regularization leads to a 'locked' model with suppressed variation. On the other hand, the model that is allowed to have larger V_S variation (relaxed model) (red line and dot) is supposed to better explain the data with less well determined model parameters, that is, model error 0.03 km s^{-1}. Because the initial model fits the data sufficiently well (88 per cent), the variance reductions of models A and B remain almost the same.

The finite-frequency effect localizes interstation sensitivity near station 2, or the coast of Taiwan (Fig. 5c), where the crust is of arc

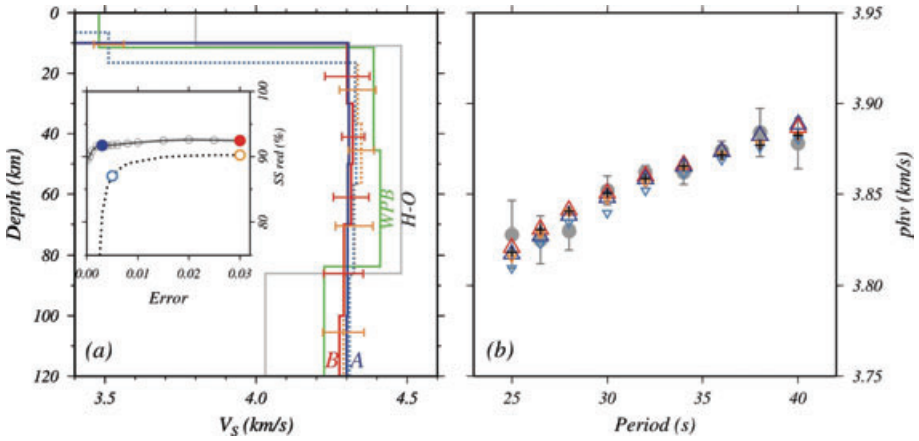

Figure 6. (a) Example V_S models for the HB and the trade-off curves of the inversion (inset). Model A with a water depth of 5 km and $h = 10$ km (blue line) is characterized by a model error of 0.003 km s^{-1} (blue filled circle) and model B (red line) by 0.03 km s^{-1} (red filled circle), and the variance, or sum of squares, reductions differ little. The counterpart models with $h = 20$ km (water depth 1.5 km) (light blue and orange dotted lines) are characterized by lower variance reductions at model errors 0.005 and 0.03 km s^{-1} (light blue and orange open circles). 95 per cent confidence intervals are plotted on each layers only for model A with $h = 10$ and 20 km. They are about ten-fold smaller for model B. The models for WPB (green line) (Kato & Jordan 1999) and Hawaii-Oahu (H-O; shaded line) (Priestley & Tilmann 1999) are shown for comparison. Depths for all models are referenced to the seafloor 5 km below the sea level. (b) Fitting of models with the phase velocity data (shaded circles with 95 per cent confidence interval). Predictions by the $h = 10$ km models are blue (A) and red (B) triangles, and those by the $h = 20$ models are light blue (A) and orange (B) inverse triangles of smaller size.

origin and may be thicker than typical HB. Noted by McIntosh *et al.* (2005), the crust may reach 20 km in thickness immediately offshore beneath the remnant Luzon arc. We test a model with $h = 20$ km and a water column of 1.5 km, representing a near-shore structure that may dominate the interstation measurement by virtue of the finite-frequency effect. The crust is composed of two 10-km-thick layers with velocities 3.1 and 3.5 km s^{-1}, respectively, that are averaged to 3.3 km s^{-1} as for $h = 10$ km. Two models were chosen from a series of inversions in the same manner as above. The reduced water column slightly compensates the thickened crust, and the net effect is a slightly higher V_S at shallow mantle depths than with $h =$ 10 km. The 'locked' model explains 83 per cent of the data, while the 'relaxed' model achieves a 91 per cent fit with a more flexible shallow mantle V_S. They are also referred to as models A and B but with $h = 20$ km.

The 40 s cut-off, corresponding to a wavelength approaching the interstation distance, is a subjective choice to ensure rejecting as much of unreliable measurements at longer periods as possible. In some studies, such as Yao *et al.* (2006), the limit of period extends to a wavelength twice of the interstation distance (double-distance or half-wavelength criterion). We conduct inversions with a longer dispersion curve including the dramatic fall-off at 40–50 s. In this test, we adopt the same layering as in previous experiments but extend the bottom of the model to 400 km. The V_S is allowed to adjust until below 190 km where V_S is fixed at 3.8 km s^{-1}. Bottom velocities higher than 3.8 km s^{-1} do not effectively bend the curve down to nearly match the data. In this effort, inversions only with the same a priori model error equivalent to 0.03 km s^{-1} were performed. The results are highly initial-model dependent, even after sufficient iterations, implying degraded resolvability provided by the data. Model C is inverted from a step-like structure and model D is inverted from a more complicated V_S variation with depth, both reaching ~79 per cent variance reduction (Fig. 7). In both models, V_S in the last adjustable layer between 140 and

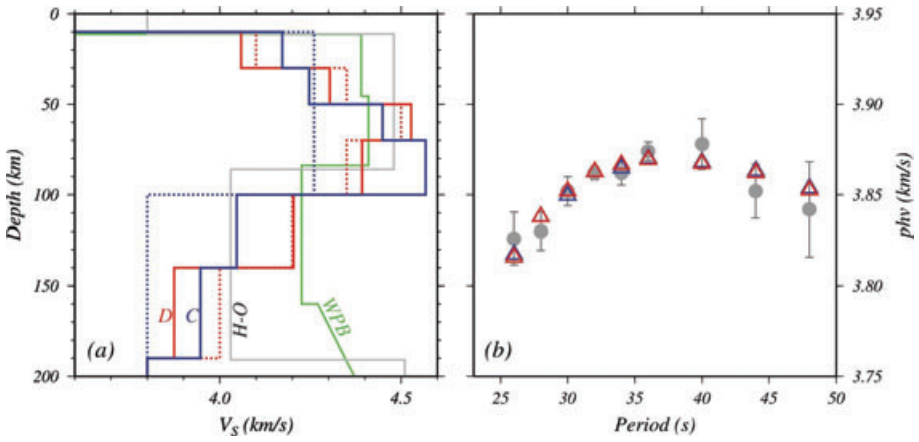

Figure 7. The same as Fig. 6 but for a dispersion data extending to 48 s and a slightly different data distribution over the period from that for 25–40 s to keep the same number of data. Trade-off curves are not shown. (a) Model C (the blue line) is inverted from a step-like initial model (blue dotted line), and model D (the red line) is inverted from a much more variable velocity distribution (red dotted line). WPB and H-O are shown for reference. (b) Predictions by models C (blue triangle) and D (red triangle). Both match ~79 per cent of the data.

190 km depths reaches a value even lower than the resolved minimum underlying the most active segment of the Hawaiian hotspot chain (Priestley & Tilmann 1999). As a consequence, V_S at lithospheric depths is increased relative to models A and B and even exceeds that of the WPB locally. However, the dramatic V_S variation over depth is dictated by the significant curvature change in dispersion beyond 40 s, for which the accuracy is questionable in the first place. These two models are considered unreliable and are discarded in favour of models A and B. The 'double-distance' or 'half-wavelength' criterion exercised in some of the previous two-station method analyses may not be a general case.

5 DISCUSSION

The exercise above illustrates how deeper structures can dictate the determination of the model parameters at all depths. At issue now is whether models A and B, inverted only from the 25 to 40 s data, are results of aliasing and biased towards lower velocities. To test this possibility, we insert low velocities with different magnitudes to model A at different depths and calculate the theoretical phase velocities in the 25–50 s range. Fig. 8 shows 2 example models (A-1 and A-2) that yield a dispersion curve flattening beyond 40 s but still fits 88 per cent of the data at 25–40 s. As expected, the calculated dispersion curve falls in between that of model A and the measured data. Models A1 and A2 show trade-off between the depths at which the low velocity zone tops and the magnitude of the velocity reduction for the same fit of the reliable part of the data (88 per cent at 25–40 s). This implies that the 25–40 s dispersion data can tolerate a presence of a 'reasonable' velocity reduction at bottom without having to increase the lithosphere part of model A. The dispersion of models A-1 and A-2 exhibits a moderate curvature more like typically found in Rayleigh wave studies (e.g. Nishimura & Forsyth 1988; Priestley & Tilmann 1999; Yao *et al.* 2006). Although the actual dispersion at long periods is unknown, model A seems to be the most robust representation of the HB at lithospheric depths. It is fair to compare model A with the WPB model of Kato & Jordan (1999) because the latter is also heavily damped, and the difference is $\sim$0.1 km s^{-1}. Below we try to make a sense of age out of this velocity difference based on the V_S model of the Pacific.

To roughly estimate the velocity-age relationship, we assume the representative age of each Pacific age zone of Nishimura & Forsyth (1989) to be the midrange value. The Pacific velocity-age model mainly reflects a thermal control and we extract this information from the Pacific and apply it to the Philippine Sea, which may be compositionally different from the former (Kato & Jordan 1999; Isse *et al.* 2004). This approach is justified based on the analysis that the Philippine Sea basin subsides with age at a rate statistically not different from that for the main oceanic basins (Horai 1982). In other words, thermal contraction still dominates the age-related properties of the marginal seas. The 4–20 and 20–52 age zones of the Pacific have midrange ages of 12 and 36 Ma, respectively, and the difference in V_S at lithospheric depths is approximately 0.15 km s^{-1} (Nishimura & Forsyth 1989). This amounts roughly to a 0.15 km s^{-1} difference for 24 Ma, essentially due to cooling of the upper mantle. The 20–52 and 52–110 age zones, with midranges 36 and 81 Ma, have a difference of $\sim$0.15 km s^{-1} too, yielding a rate of 0.15 km s^{-1} per 45 Ma. A 0.1 km s^{-1} difference therefore translates to age differences of 16 and 30 Ma for the two midrange age intervals. Assuming the WPB sampled by Kato & Jordan's (1999) Philippine-Japan profile has a representative age of 45–50 Ma and the HB is younger; the observed 0.1 km s^{-1} difference in V_S between HB and WPB may correspond to an age difference bounded between 16 and 34 Ma. These lead to an apparent age of 15–34 Ma for the HB. This age range is consistent with that of the PVB but depart considerably from the early Cretaceous. Note that, without sediment correction, the average seafloor depths of HB and PVB agree to within tens of metres, being on the order of 4800 m calculated from a global data set (Smith & Sandwell 1997). The correlations of depth, measured phase velocity, and ages roughly extrapolated for the HB with those of the PVB constitute a self-consistent system.

A mechanism that may lower the velocity of the HB lithosphere is that the brittle layer of the lithosphere is fractured by active collision with Taiwan. Historically, there are several events with M_b between 5.5 and 6.2 that have occurred in this part of the HB, and these sporadic, intraplate events are roughly aligned to form a fault zone trending NNE–SSW (Kao *et al.* 2000). The centroid depths determined from fitting *P* waveforms (Kao *et al.* 2000) all fall in the range of 6–11 km beneath the seafloor. The shallow depths and the moderate magnitudes both suggest that only the very shallow

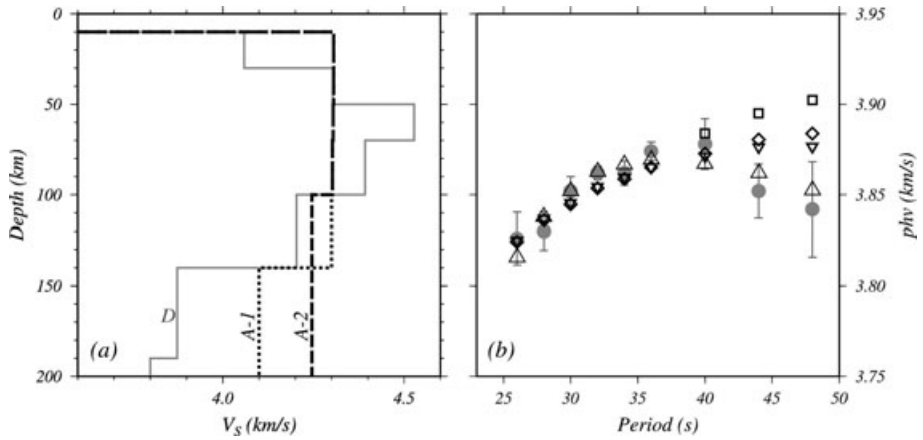

Figure 8. The same as Fig. 7 but for model A with reduced velocities at bottom. To fit data at the same 79 per cent variance reduction for 25–40 s, the low velocity zone is either deeper and stronger (A-1, dotted line) or shallower and weaker (A-2, dashed line). Model D is shown for reference. (b) The predictions of A-1 (inverse triangle) and A-2 (diamond) fall between those of model A (square, only for 40–50 s) and D (triangle), and display a moderate flattening towards long periods.

part of a spatially restricted area of the lithosphere is fractured and possibly weakened. The Rayleigh wave paths cut through this postulated fault zone at a relatively high angle, further reducing the impact of the fault zone on the propagation of the Rayleigh wave.

The phase velocity measured may not properly represent the average of HB in the presence of azimuthal anisotropy which has been repeatedly documented for the Pacific basin in the last two decades (e.g. Nishimura & Forsyth 1988; Maggi *et al.* 2006). The general conclusion is that the fast direction of vertically polarized shear wave (SV) either parallels the orientation of the fossil seafloor spreading that has been preserved in the lithosphere earlier or agrees with the direction of absolute plate motion through progressive entrainment of the asthenosphere (e.g. Maggi *et al.* 2006). The 2–3 per cent peak-to-peak variation is sufficient to explain the 0.1 km s^{-1} difference in V_S between model A ($h = 10$ or 20 km) and the WPB. As seismic anisotropy has never been explored for the HB, we generalize our Pacific experience to the HB. Because the magnetic lineaments run mostly EW (Hilde & Lee 1984; Deschamps *et al.* 2000) and the GR as a remnant fracture zone (Deschamps *et al.* 1998) is NS, the 'frozen-in' fast SV, if exists, may be aligned NS. Our NW propagating Rayleigh waves in this case sample mostly the neutral direction. The PSP motion with respect to Eurasian is NW (Seno *et al.* 1993). If the absolute plate motion dominates, the interstation Rayleigh waves travel actually along the fast direction and the V_S of HB may be overestimated relative to the average. This scenario should be less relevant in this study as model A is primarily a lithospheric model. We infer that the low phase velocity and the low V_S of the HB cannot be explained by azimuthal anisotropy in the basin.

Judging from the seismological evidence and the apparent correlation in seafloor depths, it is natural to adopt an age for the HB similar to that of the PVB. Because Isse *et al.*'s (2004) Perece-Vela measurements are more scattered than in this study, the upper bound of the age may be relaxed to 30–40 Ma. The 40 Ma agrees with the earlier results of Hilde & Lee (1984), but we tend to dismiss the palaeomagnetic age as a strong constraint because its determination could be non-unique for such a small basin. The lower bound is more arbitrary. Because the LA straddles a long distance across the basin, the basin should predate the arc. The fission-track ages of the LA, including the part that has been accreted to Taiwan, show a maximum of ∼16 Ma (Yang *et al.* 1995), and the lower bound should be somewhat older than this. From a strict geophysical point of view, the current HB may be 20–40 Ma in age. We adopt this age range as an ad-hoc, working model for further discussion.

While an evaluation of Deschamps *et al.*'s (2000) dating result is not the purpose of this study, resolving the difference between the two age models is of critical importance. Knowing better the restrictions in each of the two different approaches might be a foundation for a future effort to reconcile the discrepancy. The detailed deeper structure of the HB is much desired. With the size of the HB, however, it is probably impractical to plan for an interstation aperture much longer than used in this study. Experiments that provide a direct comparison between HB and WPB based on the same seismological observations, such as body wave traveltimes or waveforms, should be useful. Heat-flow measurements are critical to assess the thermal rejuvenation hypotheses (Deschamps *et al.* 2000). The Ar–Ar dating has developed to be a mature technique and the technical results of Deschamps *et al.* (2000) appear to be sound. However, so far the two dredging sites are located in the southeast corner of the HB. Data from more diverse sites may add more credibility to the geochronological model. Other evidence cited in

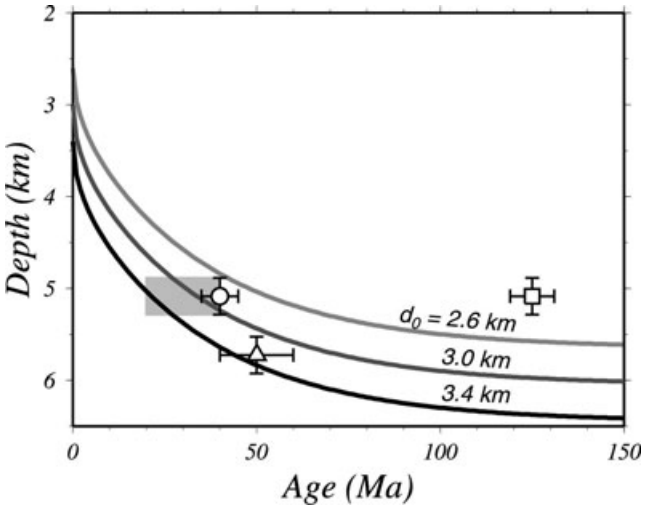

Figure 9. Seafloor depths of the HB are plotted with three age estimates: 119–131 Ma (Deschamps *et al.* 2000) (square); 40 Ma [Hilde & Lee 1984] (circles); and the *ad hoc* seismological age 20–40 Ma (this study) (shaded rectangle), in comparison with the seafloor depths of the WPB centred at about 50 Ma (triangle). The depth has been corrected for isostatic effect of sediments. The three curves are Stein & Stein's (1992) model with different axial depths d_0. Note an HB of 20–40 Ma and the WPB fit in accord with a simple model of subsidence as a function of age.

Deschamps *et al.* (2000) is the early Cretaceous fossil of radiolarians discovered in Lanyu, a small island on the Luzon volcanic arc that is in the course of collision with Taiwan. The radiolarian cherts were extracted from boulders of volcanic breccias collected in a few creek valleys, whereas chert outcrops have never been found on Lanyu (Yeh & Cheng 2001, 2009, personal communication). The possibility of the provenance of these rocks being non-*in situ* needs to be considered.

In the following we evaluate the thermal rejuvenation hypothesis to reconcile the two age models. Because the HB is on average 500–1000 m shallower than the WPB, our ad hoc model is in accord with the thermal-isostatic model of oceanic lithosphere established for oceanic basins (Fig. 9). In contrast, Deschamps *et al.*'s (2000) ages reverse the general isostatic relationship, that is, the HB is shallower despite it is much older. If the HB is indeed ∼125 Ma old, compensation mechanisms have to be at work to keep the basin afloat relative to the ∼50 Ma neighbouring WPB. If the HB crust is thickened significantly, crustal isostatic compensation would do that. However, as emphasized in McIntosh *et al.* (2005), the crust of HB along a sea–land profile almost overlapping the interstation region of this study can be considered 'normal' (<10 km) in thickness. By comparison, the thickness of the crust of WPB determined by Kato & Jordan (1999) is 11 km, which does not differ much from the norm of the oceanic crust and is very close to the 10 km assumed in the inversion above. The isostatic compensation due to crustal thickness variation would play no role in reversing the depth contrast across these two basins.

Now, if the crustal isostasy is unimportant, necessary buoyancy may be provided by thermal anomalies, for example, a thermal plume heating up the HB lithosphere in a fashion as in Hawaii. The isostatic balance requires $(\rho_{\rm m} - \rho_{\rm w}) \cdot d = -\alpha\rho_{\rm m}\Delta T \cdot H$, where $\rho_{\rm m}$ and $\rho_{\rm w}$ are densities of mantle and water, respectively, d is the uplift, α is the thermal expansitivity, ΔT is the excess temperature of the plume and H is the depth range for ΔT. Fig. 9 shows that the difference in the seafloor depth between 20–40 Ma and 125 Ma is approximately 1.3 km. To uplift the 125 Ma HB lithosphere by

1.3 km (d) to mimic an age of 20–40 Ma, the thermal buoyancy $\Delta T \cdot H$ is required to be 30 000°C-km, or 300–600°C for H of 100–50 km. If it occurs in the upper 50 km of the mantle or at lithospheric depths, it produces a ∼0.27 km s^{-1} decrease in V_S from a 125 Ma lithosphere, which is consistent with the Pacific model (Nishimura & Forsyth 1989) which predicts a drop of ∼0.3 km s^{-1} for a similar age difference. The ∼600°C thermal anomaly potentially explains the low V_S of an early Cretaceous lithosphere.

One can also imagine the low velocities in models A-1 or A-2 (Fig. 8) to represent either typical asthenosphere or part of the plume which dominates a larger depth extent with subdued temperature perturbations. No matter how the heat is distributed, it has to be restricted spatially to the HB and leave the WPB intact. The plume that elevated the seafloor by 1.3 km hypothesized here can draw comparison with the Hawaiian plume, the strongest in the world in terms of buoyancy flux (Sleep 1990), which uplifts the 90 Ma Pacific Plate to the seafloor level of 25 Ma with a 1–1.5 km topographic bulge spreading 1000 km wide (Crough 1983). Thus the small size of the HB along with the sharp boundary between HB and WPB pose a difficulty to the plume hypothesis in explaining the reversed age-depth relationship inherited from Deschamps *et al.* (2000). If this difficulty is not readily resolvable, compositional effect may be considered and evaluated in the future.

6 CONCLUSION

In the past, estimates of the age of the HB have been diverse, ranging from 40 to 125 Ma. Although indirect, seismology can play a critical role via cross-examining with better-established reference models. This study takes advantage of one OBS that was deliberately deployed to facilitate an interstation Rayleigh-wave path straddling the HB, independent of other basins of the Philippine Sea. The dispersion result indicates that the HB is comparable with the PVB whose age is 15–30 Ma. The similarity in velocity between HB and PVB is bolstered by the similarity in seafloor depth.

The finite-frequency effect was examined to demonstrate the adequacy of the Rayleigh wave two-station method in this particular tectonic setting. The inversion into V_S reveals a roughly 0.1 km s^{-1} decrease in lithosphere from that of the WPB. With an age similar to that of the PVB, the phase velocity, the V_S, and the seafloor depths of the HB relative to the neighbouring WPB and the PVB can all be explained by the simple model of thermal evolution of the oceanic upper mantle. This geophysically constrained age estimate contrasts with the early-Cretaceous age previously proposed by a geochronological study, and calls for additional evidence or better interpretations to reconcile the two.

ACKNOWLEDGMENTS

We thank Ken Peal of WHOI for his supervision in co-building broad-band OBSs with IES. The associated editor and two anonymous reviewers made critical comments that helped substantially improve the manuscript. The research is supported by the National Science Council, Taiwan, Republic of China, under grant NSC 96–2745-M-001–005.

REFERENCES

Bloch, S. & Hales, A.L., 1968. New techniques for the determination of surface wave phase velocities, *Bull. seism. Soc. Am.,* **58,** 1021–1034.

Chen, B.F., Huang, B.S. & Liang, W.T., 2004. Evidence of a slab of subducted lithosphere beneath central Taiwan from seismic waveforms and traveltimes, *Earth planet. Sci. Lett.,* **229,** 61–71.

Chou, H.C., Kuo, B.Y., Hung, S.H., Chiao, L.Y., Zhao, D.P. & Wu, Y.M., 2006. The Taiwan-Ryukyu subduction-collision complex: folding of a viscoelastic slab and the double seismic zone, *J. geophys. Res.,* **111,** B04410, doi:10.1029/2005JB003822.

Collins, J.A., Verson, F.L., Orcutt, J.A., Stephen, R.A., Peal, K.R., Wooding, F.B., Spiess, F.N. & Hildebrand, J.A., 2001. Broadband seismology in the oceans: lessons from the ocean seismic network pilot experiment, *Geophys. Res. Lett.,* **28,** 49–52.

Crough, S.T., 1983. Hotspot swells, *Ann. Rev. Earth planet. Sci.,* **11,** 165–193.

Deschamps, A. & Lallemand, S., 2002. The west Philippine basin: an Eocene to early Oligocene back arc basin opened between two opposed subduction zones, *J. geophys. Res.,* **107,** 2322, doi:10.1029/2001JB001706.

Deschamps, A., Lallemand, S.E. & Collot, J.Y., 1998. A detailed study of the Gagua ridge: a fracture zone uplifted during a plate reorganization in the mid-Eocene, *Mar. geophys. Res.,* **20,** 403–423.

Deschamps, A., Monié, P., Lallemand, S., Hsu, S.K. & Yeh, K.Y., 2000. Evidence for Early Cretaceous oceanic crust trapped in the Philippine Sea Plate. *Earth planet. Sci. Lett.,* **179,** 503–516.

Hall, R., Fuller, M., Ali, J.R. & Anderson, C.D., 1995. The Philippine Sea plate: magnetism and reconstructions, in *Active Margins and Marginal Basins of the Western Pacific,* pp. 371–403, eds Taylor, B. and Natland, J., AGU, Washington, DC.

Herrmann, R.B. & Ammon, C.J., 2004. *Computer Programs in Seismology: Surface Waves, Receiver Functions and Crustal Structure,* Saint Louis University, St. Louis, MO.

Herrin, E. & Goforth, T., 1977. Phase-matched filters: application to the study of Rayleigh waves, *Bull. seism. Soc. Am.,* **67,** 1259–1275.

Hilde, T.W.C. & Lee, C.S., 1984. Origin and evolution of the West Philippine Basin, *Tectonophysics,* **102,** 85–104.

Horai, K., 1982. A satellite altimetric geoid in the Philippine Sea, *Nature,* **299,** 117–121.

Isse, T. *et al*., 2004. Rayleigh wave phase velocity measurements across the Philippine sea from a broad-band OBS array, *Geophys. J. Int.,* **158,** 257–266.

Jolivet, L., Ishiki, N. & Rangin, C., 1989. Tectonic setting of western Pacific marginal basins, *Tectonophy.,* **160,** 23–47.

Kao, H., Huang, G.C. & Liu, C.S., 2000. Transition from oblique subduction to collision in the northern Luzon arc-Taiwan region: constraints from bathymetry and seismic observations, *J. geophys. Res.,* **105,** 3059–2079.

Kato, M. & Jordan, T.H., 1999. Seismic structure of the upper mantle beneath the western Philippine sea, *Phys. Earth planet. Inter.,* **110,** 263–283.

Landisman, M., Dziewonski, A. & Sato Y., 1969. Recent improvements in the analysis of surface wave observations, *Geophys. J. R. astr. Soc.,* **17,** 369–403.

Lee, T.Y. & Lawver, L.A., 1995. Cenozoic plate reconstruction of southeast Asia, *Tectonophys.,* **251,** 85–138.

Lin, C.R., Kuo, B.Y., Liang, W.T., Chi, W.C., Huang, Y.C., Collins, J. & Wang, C.Y., 2009. Ambient noise and teleseismic signals recorded by ocean-bottom seismometers offshore eastern Taiwan, *Terr. Atmos. Ocean.,* in press, doi:10.3319/TAO.2009.09.14.01(T).

Maggi, A., Debayle, E., Priestley, K. & Barruol, G., 2006. Azimuthal anisotropy of the Pacific region, *Earth Planet. Sci. Lett.,* **250,** 57–71.

McIntosh, K., Nakamura, Y., Wang T.K., Shih, R.C., Chen, A. & Liu, C.S., 2005. Crustal-scale seismic profiles across Taiwan and the western Philippine Sea, *Tectonophysics,* **401,** 23–54.

Nakamura, Y. & Shibutani, T., 1998. Three-dimensional shear wave velocity structure in the upper mantle beneath the Philippine sea region, *Earth Planet. Space,* **50,** 939–952.

Nishimura, C.E. & Forsyth, D.W., 1988. Rayleigh wave phase velocities in the Pacific with implications for azimuthal anisotropy and lateral heterogeneities, *Geophys. J. R. astr. Soc.,* **94,** 479–501.

Nishimura, C.E. & Forsyth, D.W., 1989. The anisotropic structure of the upper mantle in the Pacific, *Geophys. J. Int.,* **96,** 203–229.

Oda, H. & Senna, N., 1994. Regional variation in surface wave group velocities in the Philippine Sea, *Tectono.,* **233,** 265–277.

Okino, K., Kasuga, S. & Ohara, Y., 1998. A new scenario of the Parece Vela basin, *Mar. geophys. Res.,* **20,** 21–40.

Okino, K., Ohara, Y., Kasuga, S. & Kato, Y., 1999. The Philippine Sea: new survey results reveal the structure and the history of the marginal basins, *Geophys. Res. Lett.,* **26,** 2287–2290.

Priestley, K. & Tilmann, F., 1999. Shear-wave structure of the lithosphere above the Hawaiian hot spot from two-station Rayleigh wave phase velocity measurements, *Geophys. Res. Lett.,* **26,** 1493–1496.

Sdrolias, M., Roest, W.R. & Muller, R.D., 2004. An expression of Philippine Sea plate rotation: the Parece Vela and Shikoku basins, *Tectonophys.,* **394,** 69–86.

Seno, T., Stein, S. & Cripp, A.E., 1993. A model for the motion of the Philippine Sea plate consistent with NUVEL-1 and geological data, *J. geophys. Res.,* **98,** 17 941–17 948.

Sleep, N.H., 1990. Hotspots and mantle plumes: some phenomenology, *J. geophys. Res.,* **95,** 6715–6736.

Smith, W.H.F. & Sandwell, D.T., 1997. Global seafloor topography from satellite altimetry and ship depth soundings, *Science,* **277,** 1957–1962.

Song, T.R. & Helmberger, D.V., 2007. P and S waveform modeling of continental sub-lithospheric detachment at the eastern edge of the Rio Grande rift, *J. geophys. Res.,* **112,** B07319, doi:10.1029/2007JB004942.

Spetzler, J., Trampert, J. & Snieder, R., 2002. The effect of scattering in surface wave tomography, *Geophys. J. Int.,* **149,** 755–767.

Stein, C.A. & Stein, S., 1992. A model for the global variation in oceanic depth and heat flow with lithospheric age, *Nature,* **359,** 123–129.

Thomson, C.J., 1997. Modeling surface waves in anisotropic structures I. Theory, *Phys. Earth planet. Inter.,* **103,** 195–206.

Wang, T.K., Lin, S.F., Liu, C.S. & Wang, C.S., 2004. Crustal structure of the southernmost Ryukyu subduction zone: OBS, MCS and gravity modeling, *Geophys. J. Int.,* **157,** 147–163.

Woods, M.T. & Okal, E.A., 1996. Rayleigh-wave dispersion along the Hawaiian swell: a test of lithospheric thinning by thermal rejuvenation at a hotspot, *Geophys. J. Int.,* **125,** 325–339.

Yang, T.F., Tien, J.L., Chen, C.H., Lee, T. & Punongbayan, R.S., 1995. Fission-track dating of volcanics in the northern part of the Taiwan-Luzon arc: eruption ages and evidence for crustal contamination, *J. SE Asian Earth Sci.,* **11,** 81–93.

Yang, Y. & Forsyth, D.W., 2006. Regional tomographic inversion of the amplitude and phase of Rayleigh wave with 2-D sensitivity kernels, *Geophys. J. Int.,* **166,** 1148–1160.

Yao, H., Van Der Hilst, R.D. & de Hoop, M.V., 2006. Surface-wave array tomography in SE Tibet from ambient seismic noise and two-station analysis-I. phase velocity maps, *Geophys. J. Int.,* **166,** 732–744.

Yeh, K.Y. & Cheng, Y.N., 2001. The first finding of early Cretaceous radiolarians from Lanyu, the Philippine sea plate, *Bull. Nat'l Museum Nat. Sci.,* **13,** 111–145.